THE JOURNAL OF PHYSICAL CHEMISTRY C

pubs.acs.org/JPCC Article

Structural Dynamics in Ionic Liquid Thin Films: The Effect of Cation Chain Length

Boning Wu, John P. Breen, and Michael D. Fayer*

Cite This: J. Phys. Chem. C 2020, 124, 4179–4189 Read Online

ABSTRACT: The structural dynamics of planar ∼100 nm thin films of three ionic liquids (ILs) were investigated using ultrafast two-dimensional infrared (2D-IR) spectroscopy. The ILs share the same anion, bis-(trifluoromethylsulfonyl)imide (NTf_2^-), but have different chain length cations: 1-butyl-3-methylimidazolium ($Bmim^+$), 1-hexyl-3-methylimidazolium ($Hmim^+$), and 1-decyl-3-methylimidazolium ($Dmim^+$). The CN stretching mode of $SeCN^-$ dissolved in the ILs served as the vibrational probe. For each IL thin-film sample, the vibrational probe cation was the same as the cation in the corresponding liquid. The films were made by spin coating the IL on CaF_2 substrates with a 100 nm silica layer on top, which was functionalized with an ionic monolayer that mimics the structure of the corresponding IL. The thicknesses of the IL films ranged from ∼50 to ∼250 nm and were controlled by the concentration of the IL in the spin-coating solution. The structural dynamics in the films are slower than those in the corresponding bulk IL, and the dynamics are slower for thinner films. Relative to the dynamics in the corresponding bulk IL, the slowing of the dynamics decreases as the cation ion alkyl chain length increases, that is, the $DmimNTf_2$ film dynamics slow down significantly less relative to bulk $DmimNTf_2$ than $BmimNTf_2$ thin films compared to bulk $BmimNTf_2$.

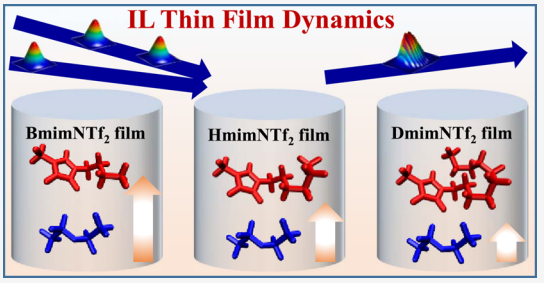

I. INTRODUCTION

Room temperature ionic liquids (ILs) are molten salts at ambient conditions. In many applications, such as catalysis, lubrication, or in electrical double-layer capacitors, the properties of an IL in close proximity to an interface play an important role. ILs have complex and varied interfacial structures.[1,2] At an IL−vacuum interface, the nonpolar alkyl chain of the cation will usually point toward the vacuum, leading to organized structures parallel to the interface.[3−13] IL−solid interfaces are more complicated because the IL structure can depend on the IL type as well as the solid substrate material and charge. There have been many studies of the structures at IL−solid interfaces using atomic force microscopy (AFM),[14−16] surface force apparatus (SFA),[17−19] X-ray and neutron reflection,[20−22] simulations,[23−27] and a variety of other methods.[28,29] These studies indicate layered structures like those reported by simulations at the IL−vacuum interface, but there is also significant inhomogeneity moving parallel to the planar interface.

The structure and dynamics of liquid molecules at interfaces are generally different from those in the bulk liquid. Liquids at interfaces, for example, water, usually display slower dynamics than those in the bulk.[30−32] The slowing at an interface will also change the dynamics of molecules close to the interface. In conventional solvents, this interfacial effect falls off over a very short distance scale. Studies of water dynamics in reverse micelles show that when water molecules are more than ∼2 nm from interfaces, they behave like bulk water.[33,34] A similar distance scale has also been observed for benzene.[35,36]

However, recent studies indicate that ILs can behave differently. In ILs, the ions that are more than 100 nm away from an interface can still be affected. Anaredy and Shaw studied vibrational spectra of nearly 1 μm thick IL films supported by a silver plate and observed different spectra than the bulk IL.[37−39] Using a confocal microscope, Ma et al. measured the relation between fluorescence anisotropy decay of fluorescent probes dissolved in ILs and distance of the probes to silica substrates.[40] Recent SFA and AFM experiments also show that ILs exhibit nonbulk behavior under nanoconfinement up to 60 nm,[41] and an IL may undergo capillary freezing under confinement larger than 100 nm.[42] The threshold size of confinement for this transition is dependent on the substrates.[42] Using ultrafast two-dimensional infrared (2D-IR) spectroscopy, it was found that the structural dynamics of ILs in the pores of polyethersulfone membranes are different from that of bulk ILs even though the average pore size was ∼350 nm.[43,44] Time-dependent fluorescent Stokes shift measurements, which report on solvation dynamics, of a coumarin probe dissolved in ILs in the ∼350

Received: December 23, 2019
Revised: January 25, 2020
Published: January 27, 2020

https://dx.doi.org/10.1021/acs.jpcc.9b11871
J. Phys. Chem. C 2020, 124, 4179−4189

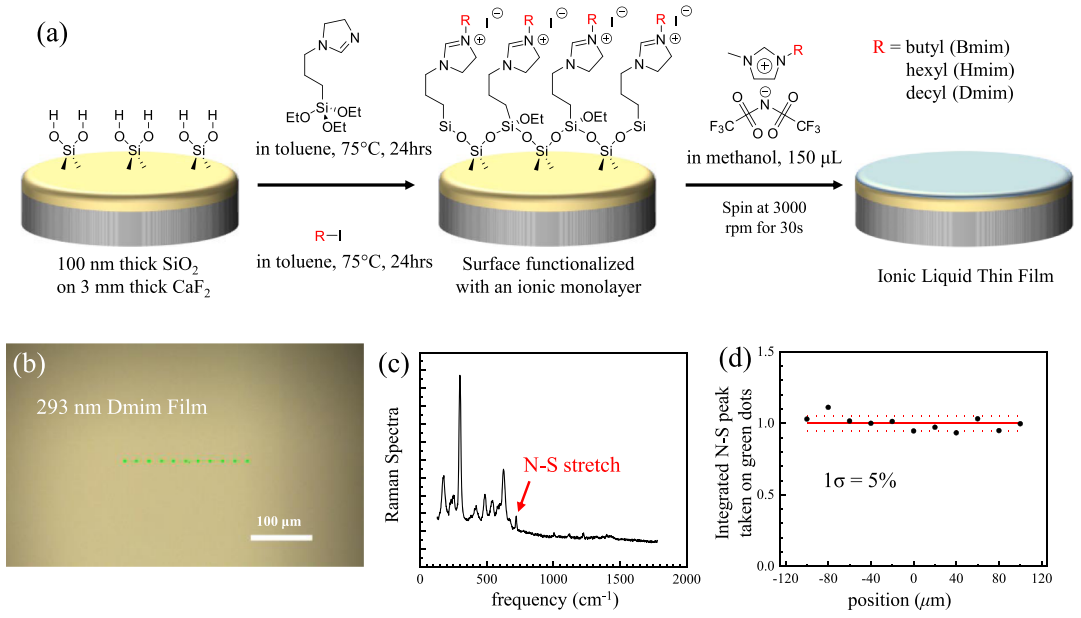

Figure 1. (a) Preparation of the IL thin films. SiO_2-coated CaF_2 windows were first functionalized with an ionic monolayer and then spin-coated with a methanol solution of the IL; (b) picture of a 293 nm $DmimNTf_2$ film; (c) Raman spectra taken on the center green spot in (b); (d) integrated intensity of N−S stretch (in NTf_2) on the green dots in (b).

nm pores of polyethersulfone membranes were also slower than in the bulk liquids, with the difference from bulk dynamics increasing for cations with shorter alkyl chains.[45] Some molecular dynamics simulations have also shown the structural changes of ILs for distances up to tens of nanometers from an interface in ILs and IL mixtures.[12,13,46]

To quantitatively investigate the influence of thin-film thickness in the ∼100 nm range, a method for making planar IL thin films was developed, and the dynamics were investigated using ultrafast 2D-IR spectroscopy.[47] The CN stretch of $SeCN^-$ dissolved in the film was used as the vibrational probe. The films were prepared by spin coating the IL 1-butyl-3-methylimidazolium bis(trifluoromethylsulfonyl)-imide ($BmimNTf_2$) on an SiO_2 layer on a CaF_2 window. The SiO_2 was functionalized with an ionic monolayer that mimics the structure of the $Bmim^+$ cation.[48] The thickness of the films was controlled quantitatively by changing the concentration of the IL in the methanol solution used for spin coating. Dramatic changes in dynamics were observed as a function of film thickness.

In this paper, we present a study of the influence of the alkyl chain length on the IL dynamics in thin films as a function of thickness. The ILs are 1-alkyl-3-methylimidazolium bis-(trifluoromethylsulfonyl)imide and the alkyl chains are butyl ($BmimNTf_2$), hexyl ($HmimNTf_2$), and decyl ($DmimNTf_2$). As mentioned above, the chain length dependence of the time-dependent Stokes shift of a coumarin probe dissolved in ILs in the ∼350 nm pores of polyethersulfone membranes was studied.[45] The results showed that the effect of confinement in the pores decreased relative to the same measurements on the bulk liquids as the length of the alkyl chain was increased. However, the broad polydispersity (∼100−500 nm) and the irregularity of the pore structure did not permit quantitative examination of the influence interface on IL dynamics. Here, by using planar thin films with various thicknesses, the influence of chain length on dynamics can be quantified.

The 2D-IR method[49,50] has been widely used to study the properties of ILs.[51−56] The 2D-IR measures spectral diffusion, and the time evolution of the vibrational frequencies of the vibrational probe molecules within the inhomogeneously broadened absorption line. Three input pulses with time separations τ between pulses 1 and 2, and T_w between pulses 2 and 3, give rise to a fourth pulse, the vibrational echo, which is the heterodyne-detected signal. Qualitatively, the experiment works as follows. Pulse 1 labels the frequencies of the probes across the inhomogeneously broadened absorption spectrum. Pulse 2, a short time later, stores the information. The system, in this case a thin IL film, is allowed to structurally evolve for the "waiting" time, T_w. Then, pulse 3 initiates a readout, and the echo pulse reports on the probe frequencies after the evolution time T_w. During T_w, the liquid structure evolves, causing the local environments of the vibrational probes to change, which in turn changes the probe frequencies. 2D spectra are recorded as a function of T_w. As T_w increases, the shape of the 2D spectra changes because the final frequencies differ more and more from the initial frequencies. The frequencies change because the structure changes. Therefore, measuring the T_w-dependent changes in frequencies reports on the structure evolution of the IL.

The T_w-dependent 2D-IR data are analyzed to obtain the frequency−frequency correlation function (FFCF), which is the connection between the experimental observables and the molecular level dynamics. An analytical theoretical model is presented that enables a reasonable determination of the correlation length of the influence of the interface on the IL dynamics. The correlation length is the decay constant in the exponential fall of the influence of the surface on the IL dynamics in a model discussed in detail below. The exponential falloff is built into the FFCF and used to fit the data. It is found that the correlation lengths for the different liquids are in the range of tens of nanometers and that the influence of the interface falls off faster (shorter correlation length) for longer cation alkyl chains.

https://dx.doi.org/10.1021/acs.jpcc.9b11871
J. Phys. Chem. C 2020, 124, 4179−4189

II. EXPERIMENTAL PROCEDURES

A. Sample Preparation. In previous reports, IL ultrathin films of a few IL monolayers were prepared using ultra-high-vacuum physical vapor deposition methods on metal surfaces.[11,57−62] Thick IL films, up to several thousand nanometers, were made on silver substrates by spin coating[63] or dynamics wetting methods.[37−39] In some studies, IL films, up to a few monolayers thick, were made on mica,[64−66] but when the film was thicker than a few monolayers, it turned into droplets.[67] There are also reports that IL films were made on alumina using vapor deposition[68] and on Si(111) using spin coating methods.[69] Attempts to form IL films on sapphire, mica, amorphous silica, and oxidized Si(110) were also made, but IL droplets were observed instead of flat films.[70−72]

Here, spin coating on surface-functionalized SiO_2 was employed to make films of controlled thickness.[47] The following materials were used. One inch diameter CaF_2 windows coated with a 100 nm layer of SiO_2 on one surface were purchased from New Wave Optics. Triethoxy-3-(2-imidazolin-1-yl)propylsilane (97%), 1-iodobutane (99%), 1-iodohexane (98%), and 1-iododecane (98%) were purchased from Sigma-Aldrich. ILs $BmimNTf_2$, (99%), $HmimNTf_2$ (99%), and $DmimNTf_2$ (99%) were purchased from IoLiTec. 1-Butyl/hexyl/decyl-3-methylimidazolium selenocyanate (Bmim/Hmim/Dmim SeCN) was synthesized according to a previously described method,[73] and the contents of residual potassium ions (8.9 ppm in Bmim SeCN, 21 ppm in Hmim SeCN, and 15 ppm in Dmim SeCN) in the ILs were measured using ICP−MS. Ethanol (200-Proof, 99.5%), toluene (99.9%), and methanol (extra dry, 99.8%) were from Fisher Chemicals. The ILs were dried under 100 mTorr vacuum for 48 h and kept inside a nitrogen-purged glovebox before use.

The procedure for making IL thin films is shown in Figure 1. Figure 1a illustrates the chemical steps. A CaF_2 window with a 100 nm layer of SiO_2 on one side undergoes a surface functionalization, turning the surface-terminal OH groups into an ionic monolayer to enhance the affinity between the solid surface and IL. Then, an IL thin film is spin-coated on the window. The functionalization contains two steps, each of which involves immersing the window into a 0.03 M toluene solution and then heating at 75 °C for 24 h. The chemical used in step 1 is triethoxy-3-(2-imidazolin-1-yl)propylsilane and that in step 2 is iodobutane, iodohexane, or iododecane, depending on which the IL film is made. After each step, the solution is removed, the window is rinsed with toluene three times, sonicated in toluene for 5 min, followed by rinsing with ethanol three times, sonicating in ethanol for 5 min, and dried using a clean nitrogen gas flow. The result shows that the SiO_2 surface is functionalized with alkyl-imidazolinium cation with I^- as the anion, where the alkyl chain is butyl, hexyl, or decyl, depending on whether a $BmimNTf_2$, $HminNTf_2$, or $DmimNTf_2$ film is being made.

To make an IL thin film on the window, 150 μL of methanol solution of the desired IL is dropped on the center of the window and then the window is spun at 3000 rpm for 30 s. The film thickness depends on the concentration of the precursor methanol solution. Figure S4 in the Supporting Information shows the correlation between film thickness and precursor solution concentration. The samples were prepared in a nitrogen-purged glovebox, where the water and oxygen levels are below 0.5 and 5 ppm, respectively.

For the 2D-IR experiments, $SeCN^-$ is added to the ILs as the vibrational probe by dissolving 10% (molar ratio) Bmim/Hmim/Dmim SeCN in the corresponding IL, before making the precursor methanol solution. It is important to note that with the addition of the vibrational probe, the cation is the same as the IL; only the anion is different. Previously, a detailed concentration study of the dynamics of the bulk IL was performed, and it was determined that a 10% molar ratio did not change the spectral diffusion dynamics.[47] To confirm that a 10% concentration does not influence the dynamics in films, a study was performed on a film using 4% probe concentration. The measured dynamics were identical. Details and data are presented in the Supporting Information. The lack of concentration dependence also demonstrates that there is no significant difference in the probe concentration at the surface that contributes to the surface effect on film dynamics. The thin films are sealed in a sample cell under a N_2 atmosphere by stacking a 1 in. O-ring and another CaF_2 window on top of the spin-coated window.

The Fourier transform infrared (FT-IR) spectra of the samples were measured using a Thermo Scientific Nicolet 6700 FT-IR spectrometer. FT-IR spectra are used to determine the thickness of the films, by comparing aromatic C−H stretch absorptions between 3070 and 3210 cm^{-1} (C−H stretching modes of the imidazolium ring) in the films with a bulk sample that has known thickness.

A Horiba XploRA Confocal Raman microscope was used to characterize the flatness of films. Pictures of the films were taken under a visible microscope using a 10× objective. Then, a 532 nm green laser is used to excite the sample, and the Raman signal emitted from the laser spot focused on the sample was collected by the confocal microscope with a 100× objective. The sample was scanned laterally with a step size of 20 μm for a total length of 200 μm. The N−S stretch signal from NTf_2 at 740 cm^{-1} was measured at each spot to evaluate the variation in the sample thickness. Figure 1b shows a picture of a 293 nm $DmimNTf_2$ film viewed with the visible microscope. No lateral structure can be seen in the image, indicating that a flat and homogeneous thin film is obtained. Figure 1c shows the local Raman spectrum on the central green dot in Figure 1b obtained using the confocal microscope. The peaks below 700 cm^{-1} arise from the substrate, and the small peaks above 700 cm^{-1} are IL peaks. The strongest IL peak at 740 cm^{-1}, which is assigned to N−S stretch in NTf_2^-, was integrated for each green dot in the picture and plotted in Figure 1d. The small variation in the N−S signal intensity for different spots confirms the uniformity of the film. When a dust particle falls on the film, the IL will aggregate around it. In the IR experiments, we were unlikely to encounter a dust spot because the films were made in a glovebox and dust particles are rare. Bad spots on a sample were further avoided by checking the signal variation from on spot to another on a sample, as well as picking spots that exhibited very little scattered light. The pictures and Raman spectra of other $HmimNTf_2$ and $DmimNTf_2$ films with different thicknesses are available in the Supporting Information. Thinner films have larger percentage thickness variation, which is mainly due to surface variations of the substrates and some measurement variation due to the larger random noise in Raman spectra when the signal is small. As we have shown previously and discussed below in the theoretical model, the thickness variation does not significantly affect the measured dynamics.[47]

https://dx.doi.org/10.1021/acs.jpcc.9b11871
J. Phys. Chem. C 2020, 124, 4179−4189

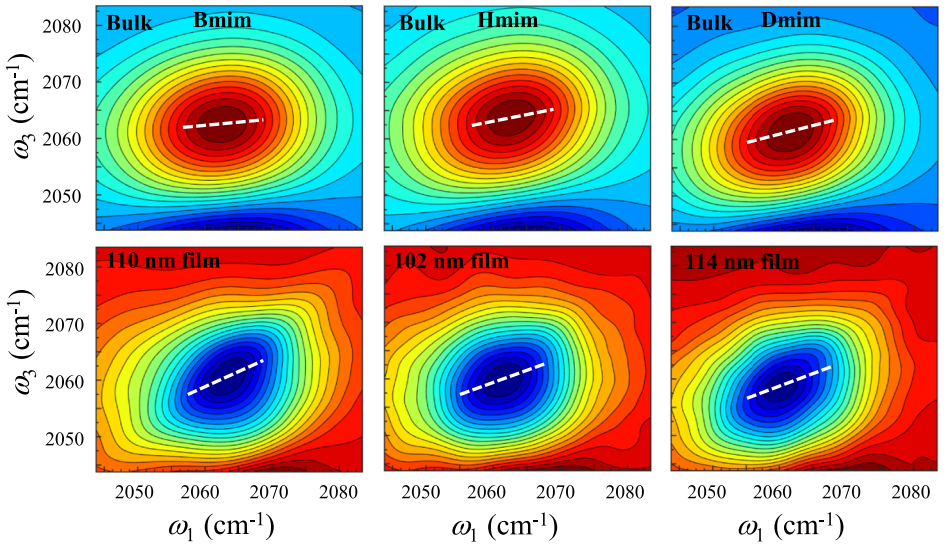

Figure 2. 2D-IR spectra of bulk (top) and films (bottom) of Bmim (left), Hmim (middle), and Dmim (right).

B. 2D-IR Spectroscopy. The 2D-IR spectra were measured using the same instrumentations as has been described previously.[47] IR laser pulses were generated at 3 kHz repetition rate by a Ti-sapphire regenerative amplifier (Spectra Physics Spitfire Ace) pumped by an oscillator (Spectra Physics Mai Tai SP). The emitted laser pulses were directed into a home-built multistage optical parametric amplifier to obtain mid-IR; the wavelength is centered at 2063 cm^{-1}. The duration and the bandwidth of the pulses were 165 fs and 90 cm^{-1} full widths at half-maximum. A 2D-IR spectrometer based on a germanium acousto-optic modulator pulse shaping system was used to perform the experiments.[74] The delay time, τ, between the phases of the first two pulses was controlled using the pulse shaper, and the delay time between pulse 2 and pulse 3 (the probe pulse) was controlled with a long mechanical delay line. The first two pulses, which are collinear, are set to vertical polarization (s-polarization), while pulse 3 is horizontally polarized (p-polarization). The 2D-IR vibrational echo signal is collinear with excitation pulse 3, and pulse 3 also acts as the self-heterodyned local oscillator (LO). The combined signal/LO is steered into a monochromator acting as a spectrograph, and a 32-pixel MCT array detector was used to observe the heterodyne-detected signal as a function of frequency.

The 2D-IR spectra of the thin films were measured with the near-Brewster angle reflection geometry method,[47,75] in which pulse 3 (the probe pulse) had an incident angle of 52° on sample and the reflected combined signal/LO is sent into the monochromator array detector. Compared to the transmission geometry, the echo signal modulation of the LO, which is the observable, was enhanced by at least a factor of 30 with the reflection geometry. Such enhancement is necessary to acquire the weak signals from the very thin films.

Both the FT-IR and 2D-IR spectrometers were purged with water and CO_2-free air. Every thin-film sample was checked with a microscope to confirm its uniformity after the 2D-IR measurements were performed.

As discussed briefly in the Introduction section, the 2D-IR vibrational echo experiment measures spectral diffusion, which is caused by the time-dependent frequency fluctuations of the vibrational mode of the probe molecule, the CN stretch of $SeCN^-$, because of the structural evolution of its surrounding environment. To quantify the T_w dependence of the 2D-IR spectra to yield the spectral diffusion dynamics, the center line slope (CLS) method was used.[76,77] It has been shown that the CLS(T_w) decay is the normalized FFCF, which is the probability that the vibrational probe with a frequency at time $t = 0$ has the same frequency at a later time, averaged over all the frequencies in the inhomogeneously broadened absorption line shape.[76,77] The complete FFCF is typically modeled with the Kubo ansatz[49,78]

$$f(t) = \langle \delta\omega(0)\delta\omega(t)\rangle = \sum_i \Delta_i^2 \exp(-t/\tau_i) \quad (1)$$

where $\delta\omega(t)$ is the instantaneous frequency at time, t, while Δ_i and τ_i are the amplitude of the frequency fluctuation (contribution to the inhomogeneous line width) and time constant of the ith decay pathway, respectively. From the CLS(T_w) and the IR absorption spectrum, $f(t)$ can be determined. The extension of eq 1 to a model that includes the dependence on distance from the interface of the observed dynamics is presented below.

III. RESULTS AND DISCUSSION

Figure 2 shows 2D-IR spectra of the CN stretch of $SeCN^-$ taken at T_w = 100 ps for bulk samples (top row) and thin films of ~100 nm thickness (bottom row) for the ILs $BmimNTf_2$, $HmimNTf_2$, and $DmimNTf_2$. In these experiments, the bulk samples' 2D-IR spectra were measured in the transmission geometry where the IR incident angles were nearly normal to the sample, while the film samples were measured in the near-Brewster angle reflection geometry with a probe (pulse 3) incident angle of 52°, which is slightly smaller than the Brewster angle.[75] In the reflection geometry for angles less than Brewster's angle, the sign of the signal (negative) is opposite to that of the transmission geometry data (positive).[75]

The time evolution of the band shape is characterized by the CLS method, which is the normalized FFCF.[76,77] The CLS(T_w) is not affected by whether the measurement is made in the transmission or reflection geometries.[75] The center lines are shown as the white dashed lines on each spectrum. The CLS method works as follows.[76,77] Cuts are made through the 2D spectrum parallel to the ω_3 axis near the

https://dx.doi.org/10.1021/acs.jpcc.9b11871
J. Phys. Chem. C 2020, 124, 4179−4189

center of the spectrum for various values of ω_1. Each cut is a 1D spectrum. The frequency of the peak of each spectrum on the ω_3 axis is plotted versus ω_1. The points form a line. The slopes of the center lines for 2D spectra taken over the range of T_ws studied are plotted as a function of T_w. The slopes can range from 1 if the initial frequencies (ω_1) and the final frequencies (ω_3) are perfectly correlated to 0, when the initial and final frequencies are uncorrelated. The difference between 1 and the CLS value at T_w = 0 is a measure of the homogeneous line width.[76,77] A larger difference corresponds to a wider homogeneous line width.

When T_w is short, there is little time for structural relaxation to occur. Therefore, the final frequency is close to the initial frequency, leading to a 2D band shape elongated along the diagonal, and the CLS is close to 1. As T_w increases, the probe molecules will have experienced more different microenvironments, so the correlation between the initial and final frequencies is gradually lost and the slope approaches 0. In the top row of Figure 2 (bulk samples), the slopes at 100 ps show that the dynamics are slower (larger slope) as the alkyl chain length is increased. In the bottom row (films), for each liquid, the slopes are larger than for the corresponding bulk liquids, showing that the dynamics in the films are slower than in the bulk liquids. However, the difference between the slope in the film and in the bulk liquid is greater for shorter alkyl chain lengths.

Figure 3 displays CLS(T_w) data (points) for thin films of the three ILs for various thicknesses as well as the data for the bulk liquids. Each curve in Figure 3 is the average of three to eight

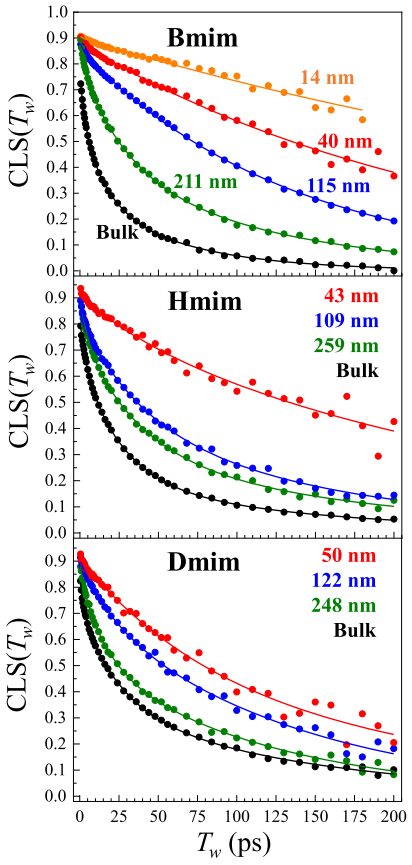

Figure 3. Averaged CLS decays in $BmimNTf_2$, $HmimNTf_2$, and $DmimNTf_2$ films, as well as the multiexponential fits.

samples. For the bulk liquids, as the alkyl chain becomes longer, the dynamics slow down, as shown by the slower decays. The chain length dependence of the dynamics of bulk methylalkylimidazoliumNTf$_2$ ILs has been studied in detail previously.[54,79] The dynamics in the films are slower than those in the bulk, and the thinner the film is, the slower its dynamics are. It is clear from inspection of Figure 3 that relative to the bulk dynamics, the slowing of the dynamics as the film becomes thinner is more pronounced as the alkyl chain length is made shorter. This trend was previously observed qualitatively using time-dependent fluorescence Stokes shift measurements on the same set of ILs confined in ~350 nm polyether sulfone membrane pores.[45]

Time-dependent CLS(T_w) decays shown in Figure 3 were fit with multiexponential functions (solid curves) in accordance with the functional form of the FFCF (eq 1). The correlation time τ_c is the integral of a decay curve and is independent of the functional form. For curves that fit with multiexponential functions, it is the sum of the amplitude weighted time constants, $\tau_c = \sum_i a_i\tau_i$. The correlation time for each film thickness was computed for each IL and divided by τ_c for the corresponding bulk liquid, $\tau_{c\text{-bulk}}$. Looking at $\tau_c/\tau_{c\text{-bulk}}$ divides out the slowing of the dynamics of the bulk liquids as the alkyl chain lengths is made longer.[79] Figure 4 displays $\tau_c/\tau_{c\text{-bulk}}$

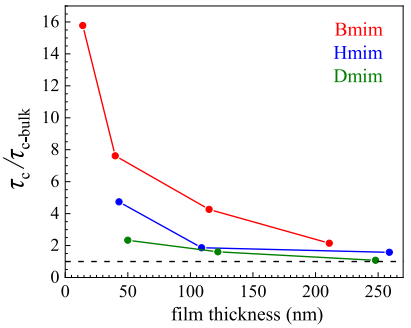

Figure 4. Correlation time in films divided by the correlation time in bulk for all three types of ILs.

versus film thickness for the three sets of different IL films. The clearest comparison is for the films that are about 45 nm thick. As can be seen in the figure, as the chain length increases, the ratio decreases. The deviation from bulk properties decreases as the chain length becomes longer. By ~250 nm, the $DmimNTf_2$ film behaves bulk like, and $HmimNTf_2$ is very close to bulk behavior. This is consistent with the measurement made on ILs in the ~350 nm pores in polyethersulfone membranes, which showed that $DmimNTf_2$ behavior had dynamics similar to the bulk liquid, while $HmimNTf_2$ displayed dynamics that were essentially within the experimental error of bulk behavior.

The results in Figure 4 show that all of the ILs have dynamics that are slow compared to bulk dynamics for thin films. The 2D-IR measurements are averages over the dynamics throughout the thickness of the film. As the film becomes thicker, a larger fraction of the IL is farther from the interfaces. The dynamics near an interface are slower, but the results indicate that the influence of the interfaces falls off faster when the alkyl chain length of the IL cation is longer. Therefore, the long alkyl chain ILs do not have to be thick before the bulk liquid far from the interface contributes such a large fraction to the 2D-IR signal, such that the measurements

https://dx.doi.org/10.1021/acs.jpcc.9b11871
J. Phys. Chem. C 2020, 124, 4179−4189

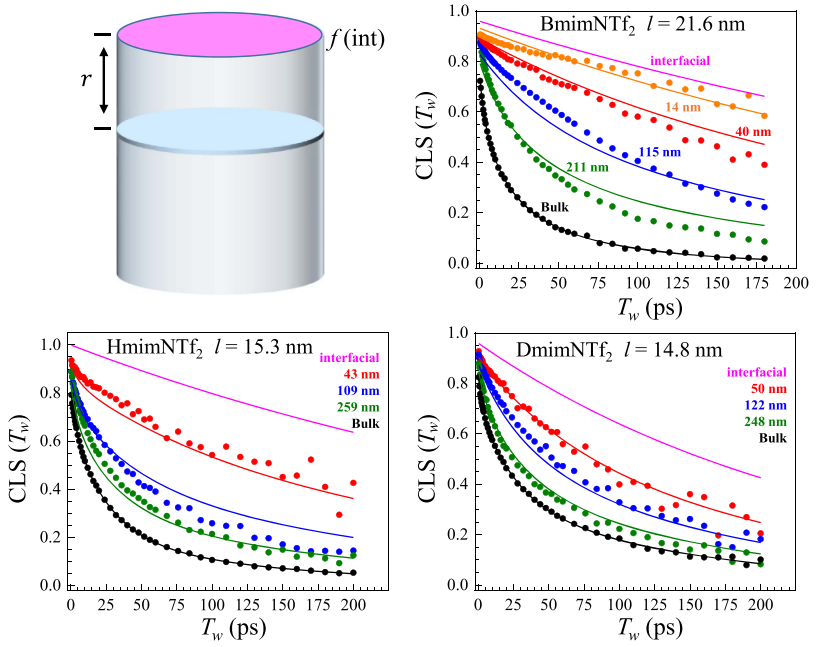

Figure 5. The theoretical model fits of the CLS decays.

report bulk dynamics. The implication is that the correlation length, the rate of falloff of the effect of the interface, is longer for short alkyl chains. In the next section, a model of the FFCF is presented, which enables the correlation length to be addressed from the experimental data.

IV. THEORETICAL MODEL AND CORRELATION LENGTH

The top left portion of Figure 5 illustrates the model for analyzing the thickness dependence of the dynamics of the IL thin films. The sample is divided into thin slices with increasing distance r from an interface. The slice right at an interface is taken to have the slowest dynamics. A slice sufficiently far from an interface has bulk dynamics. As the distance from the interface increases, the dynamics becomes faster relative to those at the interface, eventually having bulk dynamics for sufficiently large r.

In the model, the FFCF of eq 1, which is for a homogeneous liquid, is modified so that the dynamics are dependent on the distance r from the interfaces. It is assumed that the influence of an interface falls off exponentially with the distance from an interface. We have tested several functional forms for the distance dependence, including a linear decay, having a plateau where the dynamics do not change for some distance from the interface before an exponential decay, and a Gaussian decay. The linear and the Gaussian functions did not work as well. In fitting with a plateau, the width of the plateau converged to zero. The exponential distance dependence has the form

$$f(r, t) = \sum_{i=1} \Delta_i^2(r) \exp\left(-\frac{t}{\tau_i(r)}\right) \tag{2}$$

The falloff decay constant is the correlation length, l. Both the amplitudes, $\Delta_i^2(r)$, and the time constants, $\tau_i(r)$, change with the same correlation length.

Because the dynamics are slowest at the interface and become faster with increasing distance from the interface, eventually giving bulk dynamics for a thick enough sample, the time constants and the amplitudes are written as

$$\Delta_i^2(r) = (\Delta_{i,\text{int}}^2 - \Delta_{i,\text{bulk}}^2)\exp(-r/l) + \Delta_{i,\text{bulk}}^2$$
$$\tau_i(r) = (\tau_{i,\text{int}} - \tau_{i,\text{bulk}})\exp(-r/l) + \tau_{i,\text{bulk}} \tag{3}$$

where $\Delta_{i,\text{int}}^2$ and $\tau_{i,\text{int}}$ are the values of the ith amplitude and time constant, respectively, at the interface, $\Delta_{i,\text{bulk}}^2$ and $\tau_{i,\text{bulk}}$ are the values of the ith amplitude and time constant, respectively, sufficiently far from the interface to have bulk properties, and l is the correlation length. We assume that l is the same for all of the components. The experimental observable, CLS(T_w) (the normalized FFCF) as a function of T_w, is the CLS(T_w) for each slice averaged over the sample thickness, that is, averaged over all r, at time T_w. The observed CLS(T_w) for a film is the integral with respect to r over the film thickness.

$$\text{CLS}_{\text{film}}(d, T_w) = \frac{2}{d}\int_0^{d/2} \text{CLS}(r, T_w)\text{d}r$$
$$= \frac{2}{d}\sum_i \int_0^{d/2} \Delta_i^2(r)\exp\left(-\frac{T_w}{\tau_i(r)}\right)\text{d}r \tag{4}$$

where d is the total sample thickness. Note that the integral is performed from $r = 0$ to $r = d/2$ because there are two interfaces. $d/2$ is the middle of the sample. We take the effects of the two interfaces to be the same, although one interface is the functionalized SiO_2 surface and the other interface is N_2 gas. The solid surface is functionalized with alkyl-imidazolinium cations. Simulations have shown that at the IL−vacuum interface, methylalkylimidazolium cations are at the interface.[12] Therefore, the two interfacial layers in the samples studied here are likely to have a similar influence on the IL in contact with the interfaces.

The experimental CLS data from films of different thicknesses for a particular IL were fit simultaneously with eq 4. The correlation length l and the components of interfacial CLS ($\Delta_{i,\text{int}}^2$ and $\tau_{i,\text{int}}$) were floated for each IL, but they were

https://dx.doi.org/10.1021/acs.jpcc.9b11871
J. Phys. Chem. C 2020, 124, 4179−4189

shared among the different thicknesses. The parameters defining the bulk CLS(T_w) ($\Delta_{i,bulk}{}^2$ and $\tau_{i,bulk}$) were fixed to the values obtained from fitting the bulk data to a multiexponential (i.e., eq 1). The results of fitting the data with this model are shown in Figure 5, where the dots are the experimental data, and the fits are the solid curves. The pink curves in each panel are the interfacial CLS curves plotted using the parameters obtained from the fits. Given the complexity of the systems and the simplicity of the model, the model fits the data reasonably well for each IL, although the fit curves have some deviations from the data. The quality of the fits appears to improve as the alkyl chain length increases. The model provides a useful description of the data that yields the correlation length for each IL. Below, two experimental developments, which can remove systematic effects on the data, and therefore possibly improve the fits, are discussed.

The model described by eq 4 assumes that each film has a uniform thickness, that is, within the laser spot size, there is no variation in the thickness. However, in reality, the film thickness does vary above and below the average thickness, as determined by confocal Raman microscopy (see Figure 1d). The thickness variation was included in the model. The full derivation is presented in the Supporting Information. Even relatively large variations in the thickness about the average have negligible effect on the fitting results (see Fig. S1 in the Supporting Information). Therefore, for simplicity, we have not included the thickness variation in eq 4, and eq 4 was used for fitting the data.

The correlation length from the model fits are 21.6 nm for $BmimNTf_2$, 15.3 nm for $HmimNTf_2$, and14.8 nm for $DmimNTf_2$. In addition, the fits yield the dynamics of the interfacial layer (pink curves in Figure 5), which speeds up for longer alkyl chains. The combination of slower dynamics at the interface and a longer correlation length results in $BmimNTf_2$ having significantly slower dynamics relative to its bulk dynamics for a particular film thickness compared to the longer-chain ILs, $HmimNTf_2$ and $DmimNTf_2$. These results are consistent with the qualitative results from the ILs studied in the ∼350 nm pores of polyethersulfone porous membranes using the time-resolved fluorescent Stokes shift measurements discussed briefly above.[45] In those experiments, the $BmimNTf_2$ dynamics were significantly slower than the bulk dynamics in the large pores, while the $DminNTf_2$ dynamics were identical to its bulk dynamics, and $HmimNTf_2$ dynamics were exceedingly close to its bulk dynamics.

It is important to note that the correlation lengths for all three liquids are exceedingly long compared to more conventional liquids. Here, the correlation lengths are ∼20 nm. For comparison, the correlation lengths of water[33,34] and benzene[35,36] are <1 nm. For example, water in AOT reverse micelles with a radius of 2 nm has dynamics in the center region (core) of the water pool that are very close to the bulk, and larger AOT reverse micelles have bulk dynamics in their cores.[33] The long correlation length in the ILs is likely caused by charge ordering.[80] In these systems, the solid SiO_2/IL interface is lined with cations because of the surface functionalization, and simulations indicate that the gas/IL interface is also lined with cations.[5,13,46,81] The surfaces rich in cations will cause the next "layer" to be rich in anions. Given the long-range nature of the Coulomb potential, such charge ordering can extend a significant distance into the IL from each interface. This is in contrast to water molecules that have hydrogen bond interactions or benzene molecules that have van der Waals interactions, both of which are short range.

The reduction in the correlation length with increased chain length can be caused by the formation of extended alkyl region in ILs with long alkyl chains.[82,83] Calculations have shown that $Emim^+$ has the positive charge delocalized over the entire cation, including the two carbons of the ethyl group.[84] $Bmim^+$ has the two carbons at the end of the butyl chain without charge. However, ILs such as $BmimNTf_2$ do not have extended alkyl regions that percolate throughout the entire liquid.[85] Imidazolium cations with hexyl and longer chains form extended alkyl domains. For these longer-chain cations, there is a driving force for the formation of IL structures that gives rise to the extended alkyl regions. This driving force will tend to induce the IL to form its bulk structure in competition with the interface-induced layered charge ordering, which gives rise to nonbulk structure and slower dynamics near the interface. In addition, long alkyl chains must be accommodated in the interface-induced structure, making charge layers more disordered. Such an increased disorder and the tendency to form extended alkyl regions will cause the influences of the interfaces to fall off faster with distance. It is worth noting that the time-dependent fluorescence Stokes shift measurements on the $methylalkylimidazoliumNTf_2$ ILs showed that confinement in ∼350 nm pores had substantially more dynamical slowing for $Emim^+$ than for $Bmim^+$ and little or no effect on $Hmim^+$ and $Dmim^+$.

The model for the effect of film thickness on the dynamics given in eqs 3 and 4 works quite well, but clearly, the fits could be better. We are working on improving two experimental aspects of the measurements. First, the observed spectral diffusion reported by the CLS(T_w) can have two contributions, structurally induced spectral diffusion (SSD) and rotationally induced spectral diffusion (RISD).[86] SSD is caused by the structural evolution of the liquid in the vicinities of the probe molecules. It reports on the dynamics of the liquid. RISD is caused by the orientational relaxation of the probe molecules experiencing vector interactions with their environments, for example, a first-order Stark effect. As a probe molecule undergoes orientational relaxation, the Stark coupling changes causing the frequency to change. It has been shown that these two sources of spectral diffusion can be separated, so that the SSD is obtained.[86,87] To do this, it is necessary to have high-quality orientational relaxation data.[86] We have begun to develop methods to measure the orientational relaxation. Measuring orientational relaxation is done by performing polarization-selective pump−probe experiments. These measurements are actually more difficult than performing the 2D-IR experiments reported here because it is necessary to obtain the absolute amplitudes of two probe polarization configurations, parallel and perpendicular to the pump polarization. For the near-Brewster angle reflection mode necessary to obtain high-quality data, obtaining the correct polarization amplitudes is challenging.

Because we are not yet able to separate SSD and RISD, the data presented here are the combination of both.[86] Therefore, it is assumed that the correlation length for the spectral diffusion and the correlation length for the orientational relaxation are the same. This may not be true. Accurate measurements of the orientational relaxation will permit the probe orientational relaxation correlation length to be determined and the SSD to be separated from the RISD.

https://dx.doi.org/10.1021/acs.jpcc.9b11871
J. Phys. Chem. C 2020, 124, 4179−4189

The second experimental issue is nonreproducibility of the surface functionalization with alkylimidazolinium. The method of determining the film thickness is very accurate.[47] For the same film thickness prepared on different functionalized substrates, the CLS(T_w) varies to some extent. If measurements are made on a film of a given thickness, and then the IL film is removed and a new film of the same thickness is spin-coated on the functionalized substrate, the measured dynamics are the same. These observations demonstrate that the spin coating procedure and the thickness measurements are not responsible for the variation in dynamics measured for films prepared on different substrates. These results indicate that variations in the surface charge density caused by variations in the functionalization produce different dynamics. We are developing a method to reproducibly form fully functionalized surfaces. These should yield reproducible dynamics, which may eliminate some error in the thickness dependence of the data. Reproducible highly functionalized surfaces will also allow the surface charge density to be controlled by mixing chains terminated with alkylimidazolinium with just alkyl chains. Our current observations indicate that changing the surface charge density will modify the film dynamics.

V. CONCLUDING REMARKS

RTILs are being used or investigated for a wide variety of applications.[88] In many of these applications, such as electrolytes in batteries,[89,90] solvents for CO_2 capture in supported IL membranes,[91−93] media for biological studies,[94,95] and electrospray thrusters[96] and electrochemically reversible mirrors for space craft,[97] an important aspect is that the RTILs will be in contact with the interfaces.

Molecules in a liquid in contact with an interface will have distinct properties from those in the bulk liquid. The structure and dynamics of liquid molecules at an interface and for some distance beyond the layer in direct contact with an interface are distinct from those of the bulk liquid. The molecules at the interface, which will not have bulk properties that is, structural organization and dynamics, will affect the next layer of molecules further from the interface, which in turn will affect the next layer. Generally, the influence of an interface dies off rapidly. After several liquid layers, typically on a distance scale of one to several nanometers, the influence of the interface is no longer present. Molecules at interfaces typically exhibit slower structural dynamics than those in bulk liquids.[30−32] Thus, the measurement of the dynamical time scales provides a useful approach for quantifying the influence of an interface and the length scale over which the interfacial perturbation propagates. The dynamics of water molecules located within ∼1 nm from the interfaces are significantly altered, slowing substantially; however, water molecules further away from the interface, >∼3 nm, behave like those in bulk water.[33] Similar length scales have been reported in other liquid/interface systems.[35,36]

Here, using near-Brewster's angle reflection 2D-IR spectroscopy,[75] we compared the structural dynamics in the thin films of three ILs with different cation alkyl chain lengths: $BmimNTf_2$, $HmimNTf_2$, and $DmimNTf_2$. The films' thicknesses ranged from ∼14 to ∼250 nm. The surface of the SiO_2 substrate was functionalized with a cation that mimicked the particular IL that was spin-coated on the substrate to produce the thin film. The 2D-IR spectral diffusion measurements were made on the CN stretch of the vibrational probe $SeCN^-$. The results of the 2D-IR experiments showed that for all three ILs, the dynamics in the films are slower than the dynamics in the corresponding bulk liquid. In all cases, the thinner the film is, the slower the dynamics are. As shown in the plots of the correlation times for the various ILs and thicknesses (see Figures 3 and 4), longer cation ion alkyl chains yield smaller differences between the film dynamics and the bulk dynamics, that is, the slowing of the dynamics in the films relative to the bulk dynamics is in the order $BmimNTf_2$ > $HmimNTf_2$ > $DmimNTf_2$.

A theoretical model was developed to analyze the film thickness dependence quantitatively. The model assumes that the dynamics at an interface are the slowest, and as the distance from the interface increases, the influence of the interface falls off exponentially. The exponential constant that characterizes the falloff is the correlation length, l. Far from the interface, the dynamics are the same as those in the bulk IL. Fitting the data for the three ILs showed that the dynamics at the interface are slower for a shorter cation alkyl chain length. From the fits, the correlation lengths are 21.6 nm for $BmimNTf_2$, 15.3 nm for $HmimNTf_2$, and 14.8 nm for $DmimNTf_2$ (see Figure 5).

Future experiments will measure the orientational relaxation of the probe as a function of film thickness and IL type. The correlation lengths for the orientational relaxation will be compared to the correlation lengths for the IL structural dynamics. In addition, the interface will be functionalized with a vibrational probe as the head group on the surface-attached alkyl chain so that the probe is only at the interface.[98,99] The dynamics reported by 2D-IR will be measured as a function of the layer thickness and for different ILs. The experiments presented here and the future experiments will generate a detailed understanding of the nature of IL thin films.

■ ASSOCIATED CONTENT

Supporting Information

The Supporting Information is available free of charge at https://pubs.acs.org/doi/10.1021/acs.jpcc.9b11871.

Influence of thickness variation on the observed CLS dynamics of thin films; FT-IR spectra of films; relation between precursor solution and film thickness; and reproducibility of dynamics for nominally the same thickness film (PDF)

■ AUTHOR INFORMATION

Corresponding Author

Michael D. Fayer − *Department of Chemistry, Stanford University, Stanford, California 94305, United States;* orcid.org/0000-0002-0021-1815; Phone: 650 723-4446; Email: fayer@stanford.edu

Authors

Boning Wu − *Department of Chemistry, Stanford University, Stanford, California 94305, United States;* orcid.org/0000-0003-2280-3448

John P. Breen − *Department of Chemistry, Stanford University, Stanford, California 94305, United States*

Complete contact information is available at: https://pubs.acs.org/10.1021/acs.jpcc.9b11871

Notes

The authors declare no competing financial interest.

https://dx.doi.org/10.1021/acs.jpcc.9b11871
J. Phys. Chem. C 2020, 124, 4179−4189

■ ACKNOWLEDGMENTS

This work was supported by the Air Force Office of Scientific Research grant number FA9550-16-1-0104. Part of this work was performed at the Stanford Nano Shared Facilities (SNSF), supported by the National Science Foundation under award ECCS-1542152. The authors thank Dr. Jun Nishida for useful suggestions and discussions. The authors also thank Dr. Rongfeng Yuan for the help in the alignments of our laser facility.

■ REFERENCES

(1) Perkin, S. Ionic Liquids in Confined Geometries. *Phys. Chem. Chem. Phys.* **2012**, *14*, 5052−5062.
(2) Hayes, R.; Warr, G. G.; Atkin, R. Structure and Nanostructure in Ionic Liquids. *Chem. Rev.* **2015**, *115*, 6357.
(3) Lynden-Bell, R. M. Gas—Liquid Interfaces of Room Temperature Ionic Liquids. *Mol. Phys.* **2003**, *101*, 2625−2633.
(4) Santos, C. S.; Baldelli, S. Gas−Liquid Interface of Room-Temperature Ionic Liquids. *Chem. Soc. Rev.* **2010**, *39*, 2136−2145.
(5) Yan, T.; Li, S.; Jiang, W.; Gao, X.; Xiang, B.; Voth, G. A. Structure of the Liquid−Vacuum Interface of Room-Temperature Ionic Liquids: A Molecular Dynamics Study. *J. Phys. Chem. B* **2006**, *110*, 1800−1806.
(6) Lovelock, K. R. J.; Villar-Garcia, I. J.; Maier, F.; Steinrück, H.-P.; Licence, P. Photoelectron Spectroscopy of Ionic Liquid-Based Interfaces. *Chem. Rev.* **2010**, *110*, 5158−5190.
(7) Villar-Garcia, I. J.; Fearn, S.; De Gregorio, G. F.; Ismail, N. L.; Gschwend, F. J. V.; McIntosh, A. J. S.; Lovelock, K. R. J. The Ionic Liquid−Vacuum Outer Atomic Surface: A Low-Energy Ion Scattering Study. *Chem. Sci.* **2014**, *5*, 4404−4418.
(8) Nakajima, K.; Ohno, A.; Hashimoto, H.; Suzuki, M.; Kimura, K. Observation of Surface Structure of 1-Alkyl-3-Methylimidazolium Bis(Trifluoromethanesulfonyl)Imide Using High-Resolution Rutherford Backscattering Spectroscopy. *J. Chem. Phys.* **2010**, *133*, 044702.
(9) Tesa-Serrate, M. A.; Marshall, B. C.; Smoll, E. J.; Purcell, S. M.; Costen, M. L.; Slattery, J. M.; Minton, T. K.; McKendrick, K. G. Ionic Liquid−Vacuum Interfaces Probed by Reactive Atom Scattering: Influence of Alkyl Chain Length and Anion Volume. *J. Phys. Chem. C* **2015**, *119*, 5491−5505.
(10) Smoll, E. J.; Purcell, S. M.; D'Andrea, L.; Slattery, J. M.; Bruce, D. W.; Costen, M. L.; McKendrick, K. G.; Minton, T. K. Probing Conformational Heterogeneity at the Ionic Liquid−Vacuum Interface by Reactive-Atom Scattering. *J. Phys. Chem. Lett.* **2018**, *10*, 156−163.
(11) Biedron, A. B.; Garfunkel, E. L.; Castner, E. W.; Rangan, S. Ionic Liquid Ultrathin Films at the Surface of Cu (100) and Au (111). *J. Chem. Phys.* **2017**, *146*, 054704.
(12) Amith, W. D.; Hettige, J. J.; Castner, E. W.; Margulis, C. J. Structures of Ionic Liquids Having Both Anionic and Cationic Octyl Tails: Lamellar Vacuum Interface Vs Sponge-Like Bulk Order. *J. Phys. Chem. Lett.* **2016**, *7*, 3785.
(13) Hettige, J. J.; Amith, W. D.; Castner, E. W.; Margulis, C. J. Ionic Liquids with Symmetric Diether Tails: Bulk and Vacuum-Liquid Interfacial Structures. *J. Phys. Chem. B* **2017**, *121*, 174−179.
(14) Atkin, R.; El Abedin, S. Z.; Hayes, R.; Gasparotto, L. H. S.; Borisenko, N.; Endres, F. Afm and Stm Studies on the Surface Interaction of [BMP]TFSA and [Emim]TFSA Ionic Liquids with Au(111). *J. Phys. Chem. C* **2009**, *113*, 13266−13272.
(15) Hayes, R.; Borisenko, N.; Tam, M. K.; Howlett, P. C.; Endres, F.; Atkin, R. Double Layer Structure of Ionic Liquids at the Au(111) Electrode Interface: An Atomic Force Microscopy Investigation. *J. Phys. Chem. C* **2011**, *115*, 6855−6863.
(16) Atkin, R.; Borisenko, N.; Drüschler, M.; El Abedin, S. Z.; Endres, F.; Hayes, R.; Huber, B.; Roling, B. An in Situstm/Afm and Impedance Spectroscopy Study of the Extremely Pure 1-Butyl-1-Methylpyrrolidinium Tris(Pentafluoroethyl)Trifluorophosphate/Au(111) Interface: Potential Dependent Solvation Layers and the Herringbone Reconstruction. *Phys. Chem. Chem. Phys.* **2011**, *13*, 6849−6857.
(17) Perkin, S.; Albrecht, T.; Klein, J. Layering and Shear Properties of an Ionic Liquid, 1-Ethyl-3-Methylimidazolium Ethylsulfate, Confined to Nano-Films between Mica Surfaces. *Phys. Chem. Chem. Phys.* **2010**, *12*, 1243−1247.
(18) Perkin, S.; Crowhurst, L.; Niedermeyer, H.; Welton, T.; Smith, A. M.; Gosvami, N. N. Self-Assembly in the Electrical Double Layer of Ionic Liquids. *Chem. Commun.* **2011**, *47*, 6572−6574.
(19) Espinosa-Marzal, R. M.; Arcifa, A.; Rossi, A.; Spencer, N. D. Microslips to "Avalanches" in Confined, Molecular Layers of Ionic Liquids. *J. Phys. Chem. Lett.* **2014**, *5*, 179−184.
(20) Mezger, M.; Schroder, H.; Reichert, H.; Schramm, S.; Okasinski, J. S.; Schoder, S.; Honkimaki, V.; Deutsch, M.; Ocko, B. M.; Ralston, J.; Rohwerder, M.; Stratmann, M.; Dosch, H. Molecular Layering of Fluorinated Ionic Liquids at a Charged Sapphire (0001) Surface. *Science* **2008**, *322*, 424−428.
(21) Zhou, H.; Rouha, M.; Feng, G.; Lee, S. S.; Docherty, H.; Fenter, P.; Cummings, P. T.; Fulvio, P. F.; Dai, S.; McDonough, J.; Presser, V.; Gogotsi, Y. Nanoscale Perturbations of Room Temperature Ionic Liquid Structure at Charged and Uncharged Interfaces. *ACS Nano* **2012**, *6*, 9818−9827.
(22) Griffin, L. R.; Browning, K. L.; Clarke, S. M.; Smith, A. M.; Perkin, S.; Skoda, M. W. A.; Norman, S. E. Direct Measurements of Ionic Liquid Layering at a Single Mica−Liquid Interface and in Nano-Films between Two Mica−Liquid Interfaces. *Phys. Chem. Chem. Phys.* **2017**, *19*, 297−304.
(23) Shimizu, K.; Pensado, A.; Malfreyt, P.; Pádua, A. A. H.; Canongia Lopes, J. N. 2D or Not 2D: Structural and Charge Ordering at the Solid-Liquid Interface of the 1-(2-Hydroxyethyl)-3-Methylimidazolium Tetrafluoroborate Ionic Liquid. *Faraday Discuss.* **2012**, *154*, 155−169.
(24) Freitas, A. A. d.; Shimizu, K.; Smith, A. M.; Perkin, S.; Canongia Lopes, J. N. Structure and Dynamics of Mica-Confined Films of [C(10)C(1)Pyrr][NTf_2] Ionic Liquid. *J. Chem. Phys.* **2018**, *148*, 193808.
(25) Wang, Y.-L.; Laaksonen, A.; Lu, Z.-Y. Influence of Ionic Liquid Film Thickness on Ion Pair Distributions and Orientations at Graphene and Vacuum Interfaces. *Phys. Chem. Chem. Phys.* **2013**, *15*, 13559−13569.
(26) Wang, Y.-L.; Laaksonen, A. Interfacial Structure and Orientation of Confined Ionic Liquids on Charged Quartz Surfaces. *Phys. Chem. Chem. Phys.* **2014**, *16*, 23329−23339.
(27) Sha, M.; Wu, G.; Dou, Q.; Tang, Z.; Fang, H. Double-Layer Formation of [Bmim][Pf6] Ionic Liquid Triggered by Surface Negative Charge. *Langmuir* **2010**, *26*, 12667−12672.
(28) Baldelli, S. Interfacial Structure of Room-Temperature Ionic Liquids at the Solid−Liquid Interface as Probed by Sum Frequency Generation Spectroscopy. *J. Phys. Chem. Lett.* **2013**, *4*, 244−252.
(29) Wen, R.; Rahn, B.; Magnussen, O. M. In Situ Video-Stm Study of Adlayer Structure and Surface Dynamics at the Ionic Liquid/Au (111) Interface. *J. Phys. Chem. C* **2016**, *120*, 15765−15771.
(30) Singh, P. C.; Nihonyanagi, S.; Yamaguchi, S.; Tahara, T. Ultrafast Vibrational Dynamics of Water at a Charged Interface Revealed by Two-Dimensional Heterodyne-Detected Vibrational Sum Frequency Generation. *J. Chem. Phys.* **2012**, *137*, 094706.
(31) Hsieh, C.-S.; Okuno, M.; Hunger, J.; Backus, E. H. G.; Nagata, Y.; Bonn, M. Aqueous Heterogeneity at the Air/Water Interface Revealed by 2D-HD-SFG Spectroscopy. *Angew. Chem., Int. Ed.* **2014**, *53*, 8146.
(32) Yan, C.; Thomaz, J. E.; Wang, Y.-L.; Nishida, J.; Yuan, R.; Breen, J. P.; Fayer, M. D. Ultrafast to Ultraslow Dynamics of a Langmuir Monolayer at the Air/Water Interface Observed with Reflection Enhanced 2D IR Spectroscopy. *J. Am. Chem. Soc.* **2017**, *139*, 16518.
(33) Moilanen, D. E.; Fenn, E. E.; Wong, D.; Fayer, M. D. Water Dynamics in Large and Small Reverse Micelles: From Two Ensembles to Collective Behavior. *J. Chem. Phys.* **2009**, *131*, 014704.

https://dx.doi.org/10.1021/acs.jpcc.9b11871
J. Phys. Chem. C 2020, 124, 4179−4189

(34) Fenn, E. E.; Wong, D. B.; Giammanco, C. H.; Fayer, M. D. Dynamics of Water at the Interface in Reverse Micelles: Measurements of Spectral Diffusion with Two-Dimensional Infrared Vibrational Echoes. *J. Phys. Chem. B* **2011**, *115*, 11658−11670.
(35) Coasne, B.; Fourkas, J. T. Structure and Dynamics of Benzene Confined in Silica Nanopores. *J. Phys. Chem. C* **2011**, *115*, 15471.
(36) Zhu, X.; Farrer, R. A.; Fourkas, J. T. Ultrafast Orientational Dynamics of Nanoconfined Benzene. *J. Phys. Chem. B* **2005**, *109*, 12724.
(37) Anaredy, R. S.; Shaw, S. K. Long-Range Ordering of Ionic Liquid Fluid Films. *Langmuir* **2016**, *32*, 5147.
(38) Anaredy, R. S.; Shaw, S. K. Developing Distinct Chemical Environments in Ionic Liquid Films. *J. Phys. Chem. C* **2018**, *122*, 19731−19737.
(39) Anaredy, R. S.; Shaw, S. K. Directing Long-Range Molecular Ordering in Ionic Liquid Films: A Tale of Two Interfaces. *J. Phys. Chem. C* **2019**, *123*, 8975−8982.
(40) Ma, K.; Jarosova, R.; Swain, G. M.; Blanchard, G. J. Charge-Induced Long-Range Order in a Room-Temperature Ionic Liquid. *Langmuir* **2016**, *32*, 9507−9512.
(41) Jurado, L. A.; Kim, H.; Arcifa, A.; Rossi, A.; Leal, C.; Spencer, N. D.; Espinosa-Marzal, R. M. Irreversible Structural Change of a Dry Ionic Liquid under Nanoconfinement. *Phys. Chem. Chem. Phys.* **2015**, *17*, 13613.
(42) Comtet, J.; Niguès, A.; Kaiser, V.; Coasne, B.; Bocquet, L.; Siria, A. Nanoscale Capillary Freezing of Ionic Liquids Confined between Metallic Interfaces and the Role of Electronic Screening. *Nat. Mat.* **2017**, *16*, 634.
(43) Shin, J. Y.; Yamada, S. A.; Fayer, M. D. Dynamics of a Room Temperature Ionic Liquid in Supported Ionic Liquid Membranes Vs. The Bulk Liquid: 2D IR and Polarized IR Pump-Probe Experiments. *J. Am. Chem. Soc.* **2017**, *139*, 311.
(44) Shin, J. Y.; Yamada, S. A.; Fayer, M. D. Carbon Dioxide in a Supported Ionic Liquid Membrane: Structural and Rotational Dynamics Measured with 2D IR and Pump−Probe Experiments. *J. Am. Chem. Soc.* **2017**, *139*, 11222.
(45) Thomaz, J. E.; Bailey, H. E.; Fayer, M. D. The Influence of Mesoscopic Confinement on the Dynamics of Imidazolium-Based Room Temperature Ionic Liquids in Polyether Sulfone Membranes. *J. Chem. Phys.* **2017**, *147*, 194502.
(46) Jiang, W.; Wang, Y.; Yan, T.; Voth, G. A. A Multiscale Coarse-Graining Study of the Liquid/Vacuum Interface of Room-Temperature Ionic Liquids with Alkyl Substituents of Different Lengths. *J. Phys. Chem. C* **2008**, *112*, 1132.
(47) Nishida, J.; Breen, J. P.; Wu, B.; Fayer, M. D. Extraordinary Slowing of Structural Dynamics in Thin Films of a Room Temperature Ionic Liquid. *ACS Cent. Sci.* **2018**, *4*, 1065−1073.
(48) Xin, B.; Hao, J. Superhydrophobic Self-Assembled Monolayers of Long-Chain Fluorinated Imidazolium Ionic Liquids. *RSC Adv.* **2012**, *2*, 5141.
(49) Hamm, P.; Zanni, M. T. *Concepts and Methods of 2D Infrared Spectroscopy*; Cambridge University Press: Cambridge, U.K., 2011.
(50) Kraack, J. P.; Hamm, P. Surface-Sensitive and Surface-Specific Ultrafast Two-Dimensional Vibrational Spectroscopy. *Chem. Rev.* **2017**, *117*, 10623−10664.
(51) Daly, C. A.; Brinzer, T.; Allison, C.; Garrett-Roe, S.; Corcelli, S. A. Enthalpic Driving Force for the Selective Absorption of CO2 by an Ionic Liquid. *J. Phys. Chem. Lett.* **2018**, *9*, 1393−1397.
(52) Brinzer, T.; Daly, C. A.; Allison, C.; Garrett-Roe, S.; Corcelli, S. A. Modeling Carbon Dioxide Vibrational Frequencies in Ionic Liquids: Iii. Dynamics and Spectroscopy. *J. Phys. Chem. B* **2018**, *122*, 8931−8942.
(53) Yamada, S. A.; Bailey, H. E.; Tamimi, A.; Li, C.; Fayer, M. D. Dynamics in a Room-Temperature Ionic Liquid from the Cation Perspective: 2D IR Vibrational Echo Spectroscopy. *J. Am. Chem. Soc.* **2017**, *139*, 2408−2420.
(54) Tamimi, A.; Fayer, M. D. Ionic Liquid Dynamics Measured with 2D IR and IR Pump−Probe Experiments on a Linear Anion and the Influence of Potassium Cations. *J. Phys. Chem. B* **2016**, *120*, 5842.
(55) Kramer, P. L.; Giammanco, C. H.; Fayer, M. D. Dynamics of Water, Methanol, and Ethanol in a Room Temperature Ionic Liquid. *J. Chem. Phys.* **2015**, *142*, 212408.
(56) Giammanco, C. H.; Kramer, P. L.; Yamada, S. A.; Nishida, J.; Tamimi, A.; Fayer, M. D. Carbon Dioxide in an Ionic Liquid: Structural and Rotational Dynamics. *J. Chem. Phys.* **2016**, *144*, 104506.
(57) Cremer, T.; Killian, M.; Gottfried, J. M.; Paape, N.; Wasserscheid, P.; Maier, F.; Steinrück, H.-P. Physical Vapor Deposition of [Emim][Tf2n]: A New Approach to the Modification of Surface Properties with Ultrathin Ionic Liquid Films. *ChemPhysChem* **2008**, *9*, 2185.
(58) Cremer, T.; Stark, M.; Deyko, A.; Steinrück, H.-P.; Maier, F. Liquid/Solid Interface of Ultrathin Ionic Liquid Films: $[C_1C_1im]$-$[Tf_2n]$ and $[C_8C_1im][Tf_2n]$ on Au(111). *Langmuir* **2011**, *27*, 3662−3671.
(59) Schernich, S.; Kostyshyn, D.; Wagner, V.; Taccardi, N.; Laurin, M.; Wasserscheid, P.; Libuda, J. Interactions between the Room-Temperature Ionic Liquid [C2c1im][Otf] and Pd(111), Well-Ordered Al2o3, and Supported Pd Model Catalysts from IR Spectroscopy. *J. Phys. Chem. C* **2014**, *118*, 3188−3193.
(60) Rietzler, F.; Piermaier, M.; Deyko, A.; Steinrück, H.-P.; Maier, F. Electrospray Ionization Deposition of Ultrathin Ionic Liquid Films: $[C_8C_1im]Cl$ and $[C_8C_1im][Tf_2n]$ on Au(111). *Langmuir* **2014**, *30*, 1063−1071.
(61) Schernich, S.; Wagner, V.; Taccardi, N.; Wasserscheid, P.; Laurin, M.; Libuda, J. Interface Controls Spontaneous Crystallization in Thin Films of the Ionic Liquid [C2c1im][Otf] on Atomically Clean Pd(111). *Langmuir* **2014**, *30*, 6846−6851.
(62) Lexow, M.; Heller, B. S. J.; Maier, F.; Steinrück, H.-P. Anion Exchange at the Liquid/Solid Interface of Ultrathin Ionic Liquid Films on Ag(111). *ChemPhysChem* **2018**, *19*, 2978−2984.
(63) Höfft, O.; Bahr, S.; Kempter, V. Investigations with Infrared Spectroscopy on Films of the Ionic Liquid [Emim]Tf2n. *Langmuir* **2008**, *24*, 11562−11566.
(64) Beattie, D. A.; Espinosa-Marzal, R. M.; Ho, T. T. M.; Popescu, M. N.; Ralston, J.; Richard, C. J. E.; Sellapperumage, P. M. F.; Krasowska, M. Molecularly-Thin Precursor Films of Imidazolium-Based Ionic Liquids on Mica. *J. Phys. Chem. C* **2013**, *117*, 23676−23684.
(65) Wang, Z.; Priest, C. Impact of Nanoscale Surface Heterogeneity on Precursor Film Growth and Macroscopic Spreading of [Rmim]-[NTf2] Ionic Liquids on Mica. *Langmuir* **2013**, *29*, 11344−11353.
(66) Deyko, A.; Cremer, T.; Rietzler, F.; Perkin, S.; Crowhurst, L.; Welton, T.; Steinrück, H.-P.; Maier, F. Interfacial Behavior of Thin Ionic Liquid Films on Mica. *J. Phys. Chem. C* **2013**, *117*, 5101−5111.
(67) Gong, X.; Frankert, S.; Wang, Y.; Li, L. Thickness-Dependent Molecular Arrangement and Topography of Ultrathin Ionic Liquid Films on a Silica Surface. *ACS Cent. Sci.* **2013**, *49*, 7803−7805.
(68) Sobota, M.; Nikiforidis, I.; Hieringer, W.; Paape, N.; Happel, M.; Steinrück, H.-P.; Görling, A.; Wasserscheid, P.; Laurin, M.; Libuda, J. Toward Ionic-Liquid-Based Model Catalysis: Growth, Orientation, Conformation, and Interaction Mechanism of the $[Tf_2n]-$ Anion in [Bmim][Tf2n] Thin Films on a Well-Ordered Alumina Surface. *Langmuir* **2010**, *26*, 7199−7207.
(69) Carmichael, A. J.; Hardacre, C.; Holbrey, J. D.; Nieuwenhuyzen, M.; Seddon, K. R. Molecular Layering and Local Order in Thin Films of 1-Alkyl-3-Methylimidazolium Ionic Liquids Using X-Ray Reflectivity. *Mol. Phys.* **2001**, *99*, 795−800.
(70) Maruyama, S.; Takeyama, Y.; Taniguchi, H.; Fukumoto, H.; Itoh, M.; Kumigashira, H.; Oshima, M.; Yamamoto, T.; Matsumoto, Y. Molecular Beam Deposition of Nanoscale Ionic Liquids in Ultrahigh Vacuum. *ACS Nano* **2010**, *4*, 5946−5952.
(71) Liu, Y.; Zhang, Y.; Wu, G.; Hu, J. Coexistence of Liquid and Solid Phases of Bmim-Pf6 Ionic Liquid on Mica Surfaces at Room Temperature. *J. Am. Chem. Soc.* **2006**, *128*, 7456−7457.
(72) Bovio, S.; Podestà, A.; Lenardi, C.; Milani, P. Evidence of Extended Solidlike Layering in $[Bmim][NTf_2]$ Ionic Liquid Thin Films at Room-Temperature. *J. Phys. Chem. B* **2009**, *113*, 6600−6603.

https://dx.doi.org/10.1021/acs.jpcc.9b11871
J. Phys. Chem. C 2020, 124, 4179−4189

(73) Solangi, A.; Bond, A. M.; Burgar, I.; Hollenkamp, A. F.; Horne, M. D.; Rüther, T.; Zhao, C. Comparison of Diffusivity Data Derived from Electrochemical and NMR Investigations of the $SeCN^-$/$(SeCN)_2^-$/$(SeCN)_3^-$ System in Ionic Liquids. *J. Phys. Chem. B* **2011**, *115*, 6843−6852.
(74) Kumar, S. K. K.; Tamimi, A.; Fayer, M. D. Comparisons of 2D IR Measured Spectral Diffusion in Rotating Frames Using Pulse Shaping and in the Stationary Frame Using the Standard Method. *J. Chem. Phys.* **2012**, *137*, 184201.
(75) Nishida, J.; Yan, C.; Fayer, M. D. Enhanced Nonlinear Spectroscopy for Monolayers and Thin Films in near-Brewster's Angle Reflection Pump-Probe Geometry. *J. Chem. Phys.* **2017**, *146*, 094201.
(76) Kwak, K.; Park, S.; Finkelstein, I. J.; Fayer, M. D. Frequency-Frequency Correlation Functions and Apodization in Two-Dimensional Infrared Vibrational Echo Spectroscopy: A New Approach. *J. Chem. Phys.* **2007**, *127*, 124503.
(77) Kwak, K.; Rosenfeld, D. E.; Fayer, M. D. Taking Apart the Two-Dimensional Infrared Vibrational Echo Spectra: More Information and Elimination of Distortions. *J. Chem. Phys.* **2008**, *128*, 204505.
(78) Kubo, R. *Fluctuation, Relaxation, and Resonance in Magnetic Systems*; Haar, D. T., Ed.; Oliver and Boyd: London, 1962.
(79) Tamimi, A.; Bailey, H. E.; Fayer, M. D. Alkyl Chain Length Dependence of the Dynamics and Structure in the Ionic Regions of Room Temperature Ionic Liquids. *J. Phys. Chem. B* **2016**, *120*, 7488−7501.
(80) Del Pópolo, M. G.; Voth, G. A. On the Structure and Dynamics of Ionic Liquids. *J. Phys. Chem. B* **2004**, *108*, 1744−1752.
(81) Amith, W. D.; Hettige, J. J.; Castner, E. W., Jr; Margulis, C. J. Structures of Ionic Liquids Having Both Anionic and Cationic Octyl Tails: Lamellar Vacuum Interface Vs Sponge-Like Bulk Order. *J. Phys. Chem. Lett.* **2016**, *7*, 3785−3790.
(82) Castner, E. W.; Margulis, C. J.; Maroncelli, M.; Wishart, J. F. Ionic Liquids: Structure and Photochemical Reactions. *Annu. Rev. Phys. Chem.* **2011**, *62*, 85−105.
(83) Castner, E. W.; Wishart, J. F. Spotlight on Ionic Liquids. *J. Chem. Phys.* **2010**, *132*, 120901.
(84) Canongia Lopes, J. N.; Deschamps, J.; Pádua, A. A. H. Modeling Ionic Liquids Using a Systematic All-Atom Force Field. *J. Phys. Chem. B* **2004**, *108*, 2038−2047.
(85) Bodo, E.; Gontrani, L.; Caminiti, R.; Plechkova, N. V.; Seddon, K. R.; Triolo, A. Structural Properties of 1-Alkyl-3-Methylimidazolium Bis{(Trifluoromethyl)Sulfonyl}Amide Ionic Liquids: X-Ray Diffraction Data and Molecular Dynamics Simulations. *J. Phys. Chem. B* **2010**, *114*, 16398−16407.
(86) Kramer, P. L.; Nishida, J.; Fayer, M. D. Separation of Experimental 2D IR Frequency-Frequency Correlation Functions into Structural and Reorientation-Induced Contributions. *J. Chem. Phys.* **2015**, *143*, 124505.
(87) Giammanco, C. H.; Kramer, P. L.; Yamada, S. A.; Nishida, J.; Tamimi, A.; Fayer, M. D. Carbon Dioxide in an Ionic Liquid: Structural and Rotational Dynamics. *J. Chem. Phys.* **2016**, *144*, 104506.
(88) Plechkova, N. V.; Seddon, K. R. Applications of Ionic Liquids in the Chemical Industry. *Chem. Soc. Rev.* **2008**, *37*, 123.
(89) Xue, L.; Tucker, T. G.; Angell, C. A. Ionic Liquid Redox Catholyte for High Energy Efficiency, Low-Cost Energy Storage. *Adv. Energy Mater.* **2015**, *5*, 1500271.
(90) Lin, M.-C.; Gong, M.; Lu, B.; Wu, Y.; Wang, D.-Y.; Guan, M.; Angell, M.; Chen, C.; Yang, J.; Hwang, B.-J.; Dai, H. An Ultrafast Rechargeable Aluminium-Ion Battery. *Nature* **2015**, *520*, 324−328.
(91) Scovazzo, P.; Visser, A. E.; Davis, J. H.; Rogers, R. D.; Koval, C. A.; DuBois, D. L.; Noble, R. D., Supported Ionic Liquid Membranes and Facilitated Ionic Liquid Membranes.*Ionic Liquids*; American Chemical Society, 2002; Vol. *818*, pp 69−87.
(92) Lozano, L. J.; Godínez, C.; de los Ríos, A. P.; Hernández-Fernández, F. J.; Sánchez-Segado, S.; Alguacil, F. J. Recent Advances in Supported Ionic Liquid Membrane Technology. *J. Membr. Sci.* **2011**, *376*, 1−14.
(93) Dai, Z.; Noble, R. D.; Gin, D. L.; Zhang, X.; Deng, L. Combination of Ionic Liquids with Membrane Technology: A New Approach for CO_2 Separation. *J. Membr. Sci.* **2016**, *497*, 1−20.
(94) Fujita, K.; MacFarlane, D. R.; Forsyth, M. Protein Solubilising and Stabilising Ionic Liquids. *Chem. Commun.* **2005**, 4804−4806.
(95) Basu, A.; Bhattacharya, S. C.; Kumar, G. S. Influence of the Ionic Liquid 1-Butyl-3-Methylimidazolium Bromide on Amyloid Fibrillogenesis in Lysozyme: Evidence from Photophysical and Imaging Studies. *Int. J. Biol. Macromol.* **2018**, *107*, 2643−2649.
(96) Prince, B. D.; Fritz, B. A.; Chiu, Y.-H., Ionic Liquids in Electrospray Propulsion Systems. *Ionic Liquids: Science and Applications*; Amer Chem Soc: 2012 Vol. *1117*, pp 27−50.
(97) Dziedzic, R. M.; Waddington, M. A.; Lee, S. E.; Kleinsasser, J.; Plumley, J. B.; Ewing, W. C.; Bosley, B. D.; Lavallo, V.; Peng, T. L.; Spokoyny, A. M. Reversible Silver Electrodeposition from Boron Cluster Ionic Liquid (BCIL) Electrolytes. *ACS Appl. Mater. Interfaces* **2018**, *10*, 6825−6830.
(98) Yan, C.; Yuan, R.; Pfalzgraff, W. C.; Nishida, J.; Wang, L.; Markland, T. E.; Fayer, M. D. Unraveling the Dynamics and Structure of Functionalized Self-Assembled Monolayers on Gold Using 2D IR Spectroscopy and Md Simulations. *Proc. Natl. Acad. Sci. U.S.A.* **2016**, *113*, 4929−4934.
(99) Yan, C.; Yuan, R.; Nishida, J.; Fayer, M. D. Structural Influences on the Fast Dynamics of Alkylsiloxane Monolayers on SiO_2 Surfaces Measured with 2D IR Spectroscopy. *J. Phys. Chem. C* **2015**, *119*, 16811−16823.

https://dx.doi.org/10.1021/acs.jpcc.9b11871
J. Phys. Chem. C 2020, 124, 4179−4189